Title

Long-term (1980-2015) changes in net anthropogenic phosphorus inputs and riverine phosphorus export in the Yangtze River basin.

Authors

Hu, Minpeng
Liu, Yanmei
Zhang, Yufu
et al.

Publication Date

2020-06-01

DOI

10.1016/j.watres.2020.115779

Peer reviewed

Water Research 177 (2020) 115779

Contents lists available at ScienceDirect

Water Research

journal homepage: www.elsevier.com/locate/watres

Long-term (1980–2015) changes in net anthropogenic phosphorus inputs and riverine phosphorus export in the Yangtze River basin

Minpeng Hu [a], Yanmei Liu [a], Yufu Zhang [a], Hong Shen [a], Mengya Yao [a], Randy A. Dahlgren [d], Dingjiang Chen [a, b, c, *]

[a] College of Environmental & Resource Sciences, Zhejiang University, Hangzhou, 310058, China
[b] Ministry of Education Key Laboratory of Environment Remediation and Ecological Health, Zhejiang University, Hangzhou, 310058, China
[c] Zhejiang Provincial Key Laboratory of Subtropical Soil and Plant Nutrition, Zhejiang University, Hangzhou, 310058, China
[d] Department of Land, Air, and Water Resources, University of California, Davis, CA, 95616, USA

ARTICLE INFO

Article history:
Received 30 October 2019
Received in revised form
31 March 2020
Accepted 1 April 2020
Available online 6 April 2020

Keywords:
Yangtze river
Net anthropogenic phosphorus inputs
Phosphorus flux
Water quality modeling
Environmental forecasting
Nonpoint source pollution

ABSTRACT

Quantitative information on long-term net anthropogenic phosphorus inputs (NAPI) and its relationship with riverine phosphorus (P) export are critical for developing sustainable and efficient watershed P management strategies. This is the first study to address long-term (1980–2015) NAPI and riverine P flux dynamics for the Yangtze River basin (YRB), the largest watershed in China. Over the 36-year study period, estimated NAPI to the YRB progressively increased by ~1.4 times, with $NAPI_A$ (chemical fertilizer input + atmospheric deposition + seed input) and $NAPI_B$ (net food/feed imports + non-food input) contributing 65% and 35%, respectively. Higher population, livestock density and agricultural land area were the main drivers of increasing NAPI. Riverine total phosphorus (TP), particulate phosphorus (PP) and suspended sediment (SS) export at Datong hydrological station (downstream station) decreased by 52%, 75% and 75% during 1980–2015, respectively. In contrast, dissolved phosphorus (DP) showed an increase in both concentration (~7-fold) and its contribution to TP flux (~16-fold). Different trends in riverine P forms were mainly due to increasing dam/reservoir construction and changes in vegetation/land use and NAPI components. Multiple regression models incorporating $NAPI_A$, $NAPI_B$, dam/reservoir storage capacity and water discharge explained 84% and 92% of the temporal variability in riverine DP and PP fluxes, respectively. Riverine TP flux estimated as the sum of DP and PP fluxes showed high agreement with measured values ($R^2 = 0.87$, NSE = 0.84), indicating strong efficacy for the developed models. The model forecasted an increase of 50% and 7% and a decrease of 15% and 22% in riverine DP flux from 2015 to 2045 under developing, dam building, $NAPI_A$ and $NAPI_B$ reduction scenarios, respectively. This study highlights the importance of including enhanced P transformation from particulate to bioavailable forms due to river regulation and changes in land-use, input sources and legacy P pools in development of P pollution control strategies.

1. Introduction

Phosphorus (P) is an essential element for living organisms, playing a vital role in plant, food and energy production (Macintosh et al., 2018; Liu et al., 2018). To meet the enormous rise in food and energy production to sustain the increasing global population, global P inputs to the biosphere have increased four-fold over the past century (Steffen et al., 2015; Powers et al., 2016). However, increasing anthropogenic inputs cause concerns for sustainable P fertilizer supply (Yuan et al., 2018) and increasing P loads to aquatic systems that lead to water quality degradation (Vitousek et al., 2010; Goyette et al., 2018). To develop sustainable P management strategies, it is critical to quantitatively understand and characterize anthropogenic P inputs and their effects on riverine P export (Chen et al., 2018; Stackpoole et al., 2019).

Net anthropogenic phosphorus input (NAPI) is a quantitative budget approach to characterize anthropogenic P input sources, which incorporates annual P contributions from fertilizer, atmospheric deposition, seed input, non-food input (e.g., detergent P) and net import/export in animal/human food supplies (Russell

* Corresponding author. College of Environmental & Resource Sciences, Zhejiang University, Hangzhou, 310058, Zhejiang Province, China.
E-mail address: chendj@zju.edu.cn (D. Chen).

https://doi.org/10.1016/j.watres.2020.115779
0043-1354/

et al., 2008; Chen et al., 2016a). The NAPI approach was successfully applied to evaluate the impact of human activities on P balance in many watersheds across America (Russell et al., 2008; Goyette et al., 2016), Europe (Hong et al., 2017; McCrackin et al., 2018) and Asia (Han et al., 2013; Chen et al., 2015; Zhang et al., 2015).

Given the inherent relationship between NAPI and many human factors (e.g., population density, livestock density, agricultural land area), the NAPI accounting method is a powerful approach for quantitatively identifying the influence of human activities on P balance at the watershed and regional scales (Hong et al., 2012; Chen et al., 2016a). Modeling spatial or temporal variability in NAPI versus riverine P fluxes usually produces strong relationships ranging from linear (Zhang et al., 2015; Goyette et al., 2016) to exponential increases in riverine P fluxes (Chen et al., 2015, 2016a). However, the relationship varies as a function of hydroclimate, landscape use/cover, geologic/soil factors and human activities as they influence P delivery efficiency from land to water. For example, previous studies found higher fractional export of NAPI by rivers associated with higher precipitation/river discharge (Russell et al., 2008; Hong et al., 2012; Chen et al., 2015, 2016a) and greater tile drainage densities in agricultural watersheds (Han et al., 2011).

Most previous studies focused on the influence of terrestrial processes (e.g., hydroclimate and land management) on riverine P exports, while the effects of river regulation (i.e., dam/reservoir operations) received little attention. Given increasing dam/reservoir number and capacity, their impacts have altered P transport and biogeochemistry in many global watersheds (Gupta et al., 2012). For example, Beusen et al. (2016) reported retention of P by global river systems increased from 2.1 Tg yr^{-1} in 1900 to 5 Tg yr^{-1} in 2000 due to increasing dams/reservoirs. Phosphorus is easily trapped/deposited with sediments in reservoirs, but this particle-associated P may become released as more bioavailable dissolved forms by mineralization and redox alterations in the sediment layer (Eiriksdottir et al., 2017). Sediment resuspension and P release could provide a persistent source of P in aquatic ecosystems (Zhou et al., 2013). Thus, there is considerable uncertainty regarding P fate and transport dynamics resulting from reservoir impoundment (Eiriksdottir et al., 2017; Chen et al., 2018).

The Yangtze River (YRB) is the largest river in the Eurasian continent having a drainage area of 1.8×10^6 km^2 with a human population of over 4×10^8, total length of 6300 km from western to eastern China, and average annual flow of 907 km^3 yr^{-1} (Dai et al., 2011) (Fig. 1). Rapid economic development in the YRB generated 42% of China's gross domestic product, provided ~40% of grain production and supports more than 30% of China's population (Dai et al., 2011). Previous studies showed dramatic degradation of water quality in recent decades (Liu et al., 2018), with TP becoming the major pollutant concern since 2016 (Xu et al., 2018). Over the past three decades, more than 15 new large reservoirs (>1 km^3) were built along the Yangtze River and its tributaries (Yang et al., 2018).

Previous studies examined riverine P export dynamics in the YRB (Chai et al., 2009; Tong et al., 2015), finding annual/seasonal variations of P concentrations/fluxes. Additionally, modeling approaches were developed/adopted (e.g., improved export coefficient models, ENPS-LSB, WEC-DIP, Global NEWS-DIP model, IMAGE-GNM) to simulate P sources, retention and export in the YRB (Li et al., 2011; Wang et al., 2011; Shen et al., 2013; Liu et al., 2018). The impacts of dam/reservoir impoundment were poorly addressed in the majority of these modeling studies and their calibration and validation were usually limited by lack of detailed data (Wang et al., 2011; Liu et al., 2018). In contrast, NAPI-based models for riverine P export provide a simple structure to systematically incorporate human-induced P inputs with basic input data that are readily accessible. To date, there has been no attempt to apply the NAPI method in the YRB for addressing long-term P budget dynamics. A previous study successfully applied the NANI method (similar accounting approach for nitrogen) to the YRB for quantification of long-term (1980–2012) net human-induced nitrogen inputs, as well as their relationships with riverine nitrogen export (Chen et al., 2016b). Thus, the NAPI method should be effective for addressing long-term, human-induced P dynamics in the YRB.

This study used a 36-year record (1980–2015) of P sources and riverine P exports in the YRB to (i) quantify and assess the temporal and spatial dynamics of NAPI, as well as the main drivers; (ii) identify and evaluate the historical trends and influencing factors on riverine P fluxes and forms (DP, PP and TP); and (iii) develop quantitative models for simulating historical riverine P fluxes and forecasting P fluxes based on various future scenarios. This study quantitatively assessed the influence of NAPI, terrestrial biogeochemical processes, human land-use impacts and river regulation on riverine P fluxes and forms. Results of this study provide insights for guiding strategies to improve watershed P management and remediate P pollution.

2. Materials and methods

2.1. Study area

The YRB was divided into three segments (Wang et al., 2008): upstream reach (river source to Yichang), midstream reach (Yichang to Hukou) and downstream reach (Hukou to estuary) (Fig. 1). Average water discharge (Q) was 907 km^3 yr^{-1} and showed no long-term variation during the study period (Yang et al., 2018). Over the past three decades, the number of dams (capacity >0.13 km^3) within the YRB increased from 103 in 1980 to 196 in 2015 and storage capacity increased from 93 to 296 km^3 (Dai et al., 2016; Yang et al., 2018). The east branch of the "South-to-North Water Diversion Project" began in 2014 and annually transfers ~0.5 km^3 (0.03% of Q) from Jiangsu province (downstream Datong Station) to Shandong province. The middle branch of the Water Diversion Project began in 2015 and transfers 2.2 km^3 (0.2% of Q) from Danjiangkou Reservoir to Beijing and Tianjin provinces. Land-use in the YRB showed small variations from 1980 to 2010, with forest (42%), grassland (24%), farmland (27%), water area (2%), and residential land (1%) the dominant land uses as of 2010 (Table 1, Xu, 2017).

2.2. NAPI estimation and uncertainty analysis

To examine spatio-temporal variation of the anthropogenic P budget, NAPI for the YRB over 1980–2015 was determined as the sum of five major components using basic data from statistical yearbooks (Table S1): atmospheric P deposition (*APD*), chemical fertilizer P application (*CF*), net food/feed P input (*NFFI*), seed P input (*SI*) and non-food P input (*NFI*) (Russell et al., 2008; Chen et al., 2016a):

$$NAPI = CF + APD + SI + NFI + NFFI \quad (1)$$

NFFI (kg P km^{-2} yr^{-1}) was calculated as the sum of human and livestock P consumption minus the sum of P in livestock and crop production (Han et al., 2013; Chen et al., 2015):

$$NFFI = HC + AC - (G - GL) - (AP - APL) \quad (2)$$

where *HC* is human consumption, *AC* is animal consumption, *G* is harvested grain, *GL* is grain loss due to pests, spoilage and processing, *AP* is animal products, and *APL* is spoilage and inedible

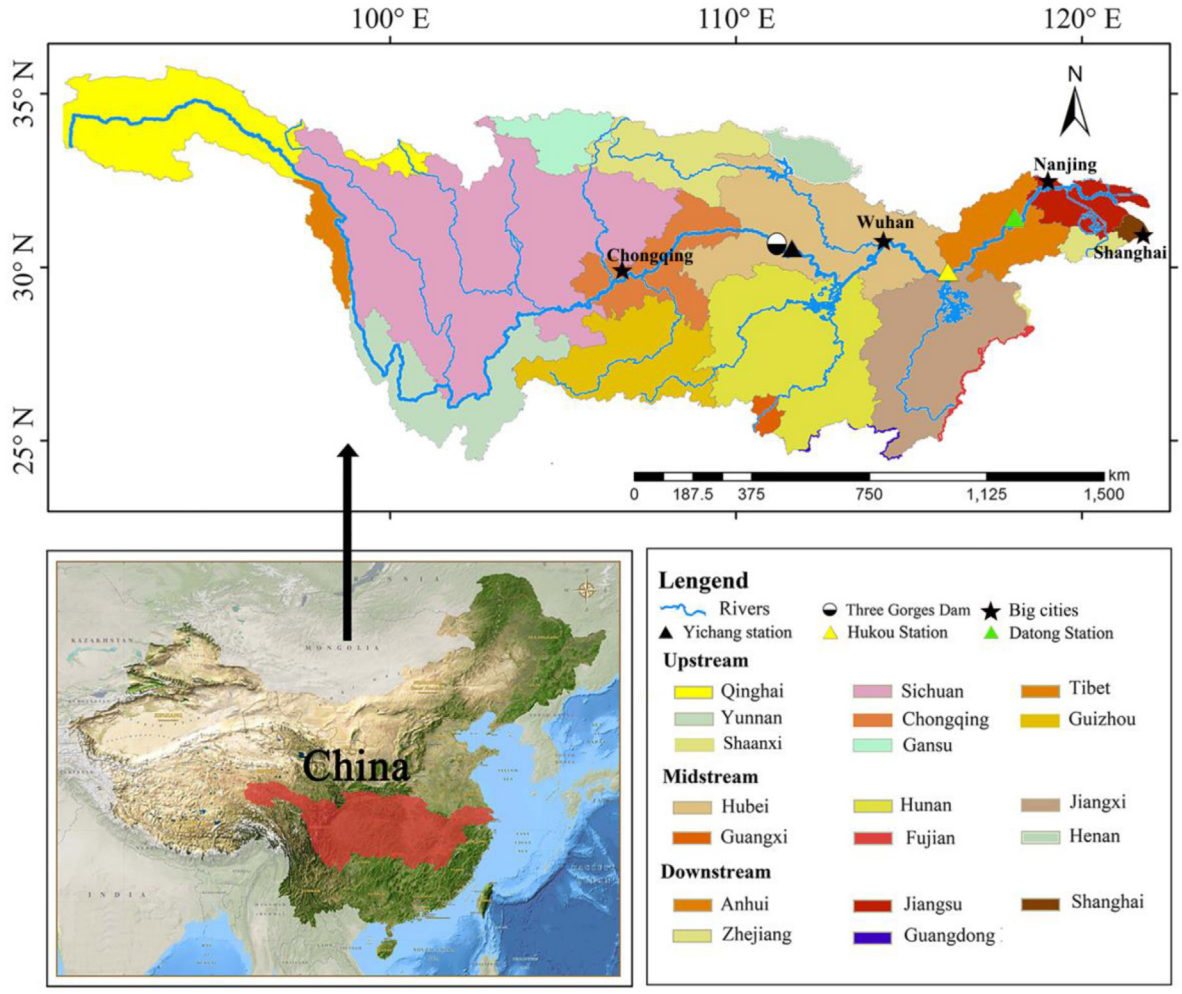

Fig. 1. Yangtze River basin and administrative divisions in China.

Table 1
Characteristics of cultivated land area, population, domestic animals, and land-use change for Yangtze River basin, 1980–2015.

	Periods	Cultivated land area percentage (%)	Population density (people km^{-2})	Animal density (number km^{-2})
Upstream (1,096,760 km^2)	1980s	8.6	134	144
	1990s	8.7	166	160
	2000s	8.6	151	184
	2010s	11.2	152	189
Midstream (589,329 km^2)	1980s	17.4	254	178
	1990s	16.7	290	250
	2000s	17.5	301	290
	2010s	19.9	314	303
Downstream (113,998 km^2)	1980s	31.7	603	292
	1990s	31.1	674	341
	2000s	30.4	757	318
	2010s	27.2	847	265
Whole basin (~1,800,000 km^2)	1980s	13.0	203	164
	1990s	12.7	239	201
	2000s	12.9	239	227
	2010s	15.0	249	232

	Period	Forest	Grass	Water area	Residential land	Unused land	Paddy field	Dry land
Whole basin (~1,800,000 km^2)	1980s	750,164	429,099	36,536	15,581	73,096	254,556	240,334
	1990s	769,449	442,946	42,945	9093	66,462	249,699	229,613
	2000s	749,332	430,242	37,740	21,336	72,759	248,643	239,285
	2010s	750,882	428,931	38,042	22,789	73,096	244,417	237,034

The land-use changes over the 1980–2015 period derived from Xu (2017) and Zhao et al. (2017).

animal products. We separated annual NAPI into $NAPI_A$ (sum of chemical fertilizer input, atmospheric deposition and seed input, implying nonpoint source pollution potential) and $NAPI_B$ (sum of net food/feed imports and non-food input, implying point source pollution potential). A detailed description of calculation methods for individual P sources and basic data sources are available in Supplementary materials (SM), Part A. We determined basin boundaries using a geographic information system with China's 1:250000 first-level watershed classification dataset from Chinese National Earth System Science Data Sharing platform. According to the administrative divisions reported in Yangtze River yearbooks, river basin boundaries are accurate down to the district and county levels.

To evaluate uncertainty in NAPI estimation and corresponding variables, we performed Monte Carlo simulations using 10,000 simulations to obtain the mean and 95% confidence interval for annual NAPI (SM, Part A2). We assumed all parameters used in estimating NAPI followed a normal distribution with a coefficient of variation of 30%, an assumption commonly used in watershed nutrient budgeting studies (Chen et al., 2019). The uncertainty estimation procedure was formulated in Microsoft Excel (2007) embedded with Crystal Ball software (Professional Edition, 2000; Oracle Ltd. USA).

2.3. Riverine P exports

Riverine P fluxes in different forms (TP-total P; PP-particulate P > 0.45 μm; DP-dissolved P < 0.45 μm) at Datong hydrological station (~640 km from ocean) were derived from published literature based on monthly/seasonally records (n ≈ 250, Dai et al., 2011; Powers et al., 2016). Yangtze River discharge varies seasonally, with more water delivery in summer (June–August) and autumn (September–November) than in winter (December–February) and spring (March–May) (Chai et al., 2009). The Datong station drainage area (~1.71×10^6 km^2) represents >95% of the total YRB area (Dai et al., 2011, 2016). We calculated riverine DP flux as the product of discharge and DP concentration at Datong station (Dai et al., 2011). Riverine DP data for 2011–2015 was estimated from the historical trend of monitoring data (1980–2010, $R^2 = 0.94$) at Datong station (Dai et al., 2011). Due to the lack of long-term field measurements for PP concentrations, we adopted the method proposed by Powers et al. (2016) to estimate the PP flux as the product of SS export values and a constant P density coefficient (0.5 g P per kg sediment) (see SM, Part B). Riverine TP flux was further defined as the summation of DP and PP fluxes (Powers et al., 2016), which produced similar historical P trends to published studies (Powers et al., 2016; Xu et al., 2018).

Other watershed characteristics, including water discharge, precipitation, SS concentration, sewage discharge and dam construction, were obtained from relevant sources reported in Table S1, SM, Part A. All correlation and regression analyses were performed using SPSS (Ver. 17.0, SPSS, Chicago, USA). One-way analysis of variance (ANOVA) was conducted to examine temporal and spatial differences in NAPI across the YRB. Regression analyses were used to determine predictive models for riverine P fluxes. The Markov Chain Monte Carlo (MCMC) method was adopted to determine uncertainty intervals for modeled riverine P yields.

3. Results

3.1. Spatio-temporal variations of NAPI

Estimated annual NAPI in YRB showed an increasing trend from 1980 to 2015 ($p < 0.001$, Fig. 2), resulting in a net increase of ~1.4-fold, with a rapid increase (944–1971 kg P km^{-2} yr^{-1}) during the first 16 years (1980–1996) and a slower increase (1971–2308 kg P km^{-2} yr^{-1}) during the 1996–2015 period (Fig. 2). Estimated $NAPI_A$ increased from 567 to 1467 kg P km^{-2} yr^{-1}, while $NAPI_B$ increased from 377 to 814 kg P km^{-2} yr^{-1} (Fig. 2). In terms of NAPI components, fertilizer input increased from 510 to 1347 kg P km^{-2} yr^{-1}, contributing 60% (52–65%) of NAPI over the 1980–2015 period. The decreasing growth rate in P fertilizer application was the primary contributor to the decreasing overall NAPI growth rate. Net food/feed P input was also an important source of NAPI, which contributed 27–39% of NAPI. Net food/feed P inputs showed an increase of ~91% (359–685 kg P km^{-2} yr^{-1}) during 1980–2015. In comparison, non-food P input increased ~8-fold during the study period (17.8–156 kg P km^{-2} yr^{-1}). Although atmospheric P deposition and seed P input only accounted for 4–6% of NAPI, their contributions to NAPI continuously increased from 1980 to 2015. Sensitivity analyses indicated NAPI values were most sensitive to fertilizer inputs, number of livestock and poultry, and animal P consumption rates (Fig. S10). Therefore, improving the accuracy of these variables/parameters would be most effective for reducing NAPI uncertainty.

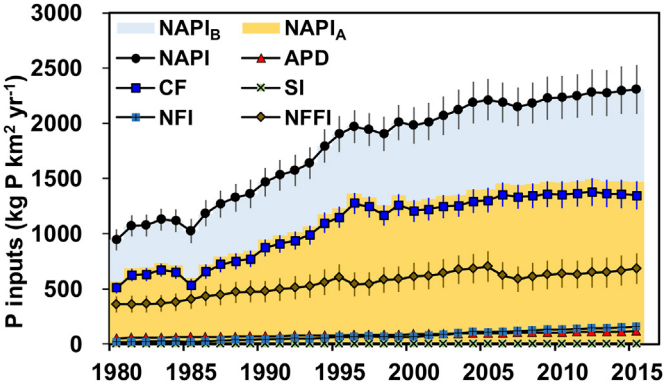

Fig. 2. Historical trends of (a) NAPI, $NAPI_A$ and $NAPI_B$ and (b) NAPI from atmospheric P deposition (APD), chemical fertilizer P input, non-food P input (NFI), net food/feed P input (NFFI), and seed P input (SI) in the Yangtze River basin over the 1980–2015 study period. Shadow area and vertical lines denote the $NAPI_A$/$NAPI_B$ components and 95% confidence intervals, respectively.

Annual NAPI in upstream and midstream watershed sections increased continuously from the 1980s–2010s, while NAPI in the downstream peaked in the 1990s, followed by a small decrease in subsequent years (Fig. 3). The highest NAPI growth rates (>2 times) were observed in Chongqing, Henan, Yunnan and Hubei (upstream and midstream provinces) from the 1980s–2010s. In contrast, NAPI growth rates were negative in Shanghai, Jiangsu and Zhejiang located in the downstream section. As for specific NAPI components, the highest growth rate for chemical fertilizer input was observed in Tibet (17.2 times), while the lowest was observed in Shanghai (−65%). The entire basin showed an increasing trend for net food/feed and non-food P inputs, with the highest growth rate in net food/feed P input (1.4 times) and non-food P input (13.3 times) observed in Yunnan and Shanghai, respectively (Figs. S7 and S8).

Multi-annual average NAPI across the YRB showed an increasing trend from west to east, with higher NAPI observed in the downstream section (3829 kg P km^{-2} yr^{-1}) compared to midstream (2477 kg P km^{-2} yr^{-1}) and upstream (983 kg P km^{-2} yr^{-1}, $p < 0.01$) (Fig. 3). The highest average NAPIs were observed in Shanghai (4613–8471 kg P km^{-2} yr^{-1}) and Henan (1250–8628 kg P km^{-2} yr^{-1}), while the lowest values were observed in Qinghai (111–167 kg P km^{-2} yr^{-1}) and Tibet (218–410 kg P km^{-2} yr^{-1}) (Fig. 3). All components of NAPI presented a similar pattern to overall NAPI, with higher values observed in downstream versus

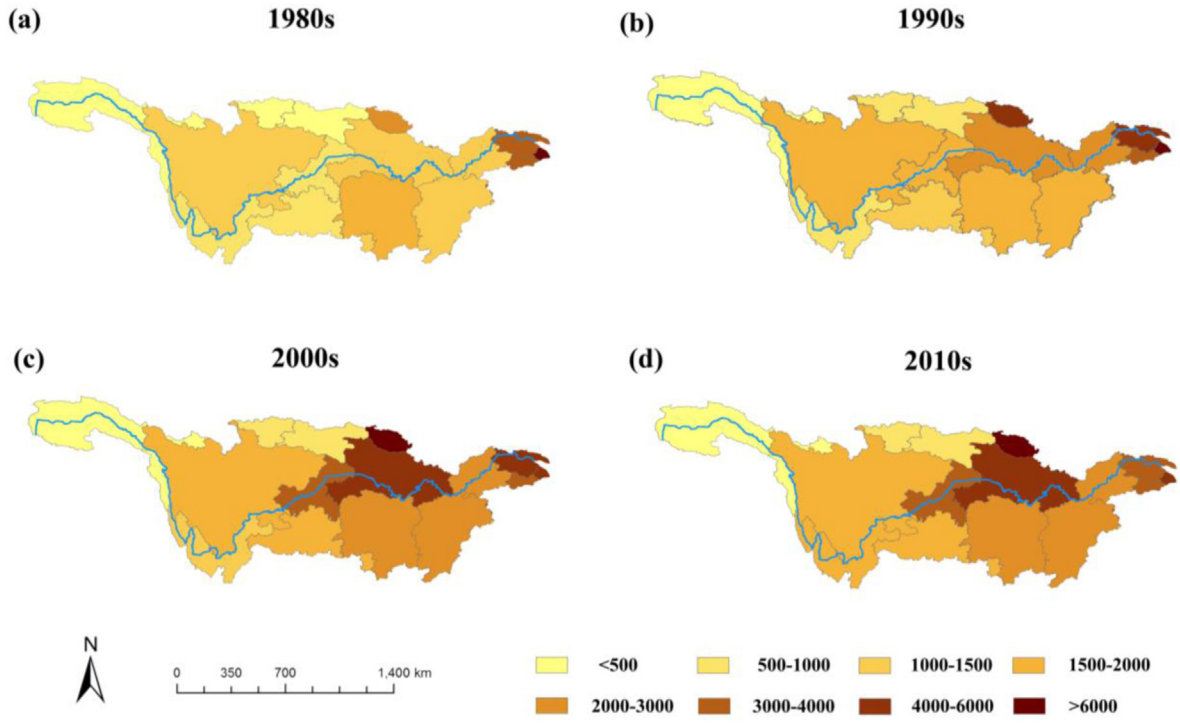

Fig. 3. Changing spatial distribution of NAPI (kg P km^{-2} yr^{-1}) in 18 provincial-level regions of the Yangtze River basin in (a) 1980s, (b) 1990s, (c) 2000s and (d) 2010s.

upstream areas (Fig. 3). The highest chemical fertilizer and seed P inputs were observed in Henan (4117 kg P km^{-2} yr^{-1}) and Jiangsu (11.9 kg P km^{-2} yr^{-1}), while the highest net food/feed and non-food P inputs were observed in Shanghai (2684 and 418 kg P km^{-2} yr^{-1}).

3.2. Drivers of spatio-temporal NAPI dynamics

Spatio-temporal differences in NAPI and its components across the YRB were mainly associated with distributions of human population and livestock densities, as well as agricultural land area. There were significant relationships between NAPI and population density and livestock density over the past 36 years, as well as across the 18 provinces in the entire YRB (Fig. 4). The high NAPI observed in Shanghai was associated with both high population and livestock densities. Despite the lower population density, a higher NAPI was observed in Henan (30–60% higher) than in Zhejiang, Jiangsu and Anhui. This results from a higher livestock density in Henan, which experienced a higher NAPI increase rate from increasing livestock density compared to changes in population density (Fig. 4c and d). Furthermore, there was a strong linear relationship between cultivated land area percentage for the 18 provinces and NAPI ($R^2 = 0.87$, $n = 18$, $p < 0.001$). Provinces with high proportions of agricultural and residential lands had the highest NAPI values, such as Shanghai, Jiangsu, Zhejiang and Anhui (downstream); Henan, Hubei and Hunan (midstream); and Chongqing (upstream) (Fig. 3).

3.3. Riverine P export dynamics

During the study period, annual riverine TP fluxes at Datong station decreased (~52%) from 142 kg P km^{-2} yr^{-1} (0.25 mg P L^{-1}) in 1980 to 68.9 kg P km^{-2} yr^{-1} (0.12 mg P L^{-1}) in 2015. PP flux accounted for 50–97% of TP flux and was therefore the primary component of riverine TP fluxes. Riverine PP flux decreased (~75%) from 137.9 to 34.3 kg P km^{-2} yr^{-1} between 1980 and 2015 (Fig. 5a). Given the strong association between PP and SS dynamics, riverine SS flux also showed a consistent decreasing trend with a net decrease of 75% from 1980 to 2015 (average SS flux of 277 tons km^{-2} yr^{-1} in 1980–1985, 199 tons km^{-2} yr^{-1} in 1986–2002, and 81 tons km^{-2} yr^{-1} in 2003–2015). In contrast, riverine DP flux increased from 4.2 to 34.6 kg P km^{-2} yr^{-1} between 1980 and 2015 (~7-fold increase) and its contribution to TP increased 16-fold (Fig. 5a).

Annual riverine TP and PP fluxes showed decreasing trends during 1980–2015 (~1.4 times, Fig. 5a) despite increasing NAPI. Negative relationships were also observed between riverine TP/PP fluxes and $NAPI_A$ or $NAPI_B$ (Table 2). The cumulative number and capacity of large dams showed a significant negative relationship with riverine TP and PP fluxes, which explained 85% of the variability in annual PP flux (Fig. 6c). In addition, hydroclimate played an important role as demonstrated by the power function relationships between discharge and TP ($R^2 = 0.31$, $p < 0.001$) and PP fluxes ($R^2 = 0.23$, $p = 0.003$).

NAPI and DP fluxes showed a positive relationship across the 36-year record ($R^2 = 0.85$, $p < 0.001$, Table 2). Strong positive relationships ($R^2 = 0.83$–0.84) between DP fluxes and $NAPI_A$ and $NAPI_B$ (Table 2) suggest an important role for both nonpoint and point source P inputs. There was no significant relationship between riverine DP flux and discharge or precipitation. Riverine DP flux was positively related to NAPI components (Table 2), with the strongest relationship associated with net food/feed input ($R^2 = 0.86$, $p < 0.001$). Similarly, increasing non-food P inputs, mainly associated with use of detergent, showed a positive relationship with riverine DP flux ($R^2 = 0.81$, $p < 0.001$, Table 2). DP flux showed a significant logarithmic relationship with dam/reservoir capacity ($R^2 = 0.66$, $p < 0.001$). Our analysis detected a temporal inflection point for the relationship between reservoir capacity and DP flux (Fig. 6b) in 2003 when Three Gorges Dam was constructed. The pre- and post-2003 segments of the relationship both showed statistically significant slope coefficients, with a weaker correlation in the 2003–2015 period ($R^2 = 0.46$, $p = 0.011$) compared to the 1980–2002 period ($R^2 = 0.80$, $p < 0.001$).

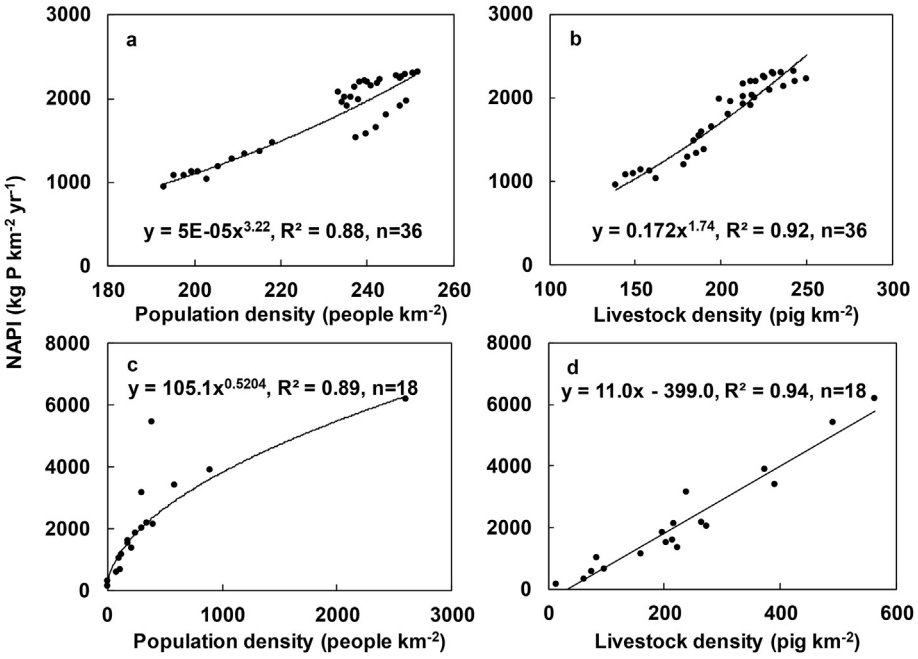

Fig. 4. Correlation ($p < 0.001$) between NAPI and (a) population density and (b) livestock density in the Yangtze River basin from 1980 to 2015. Correlation ($p < 0.001$) between average annual NAPI of 18 sub-basins and (c) population density and (d) livestock density.

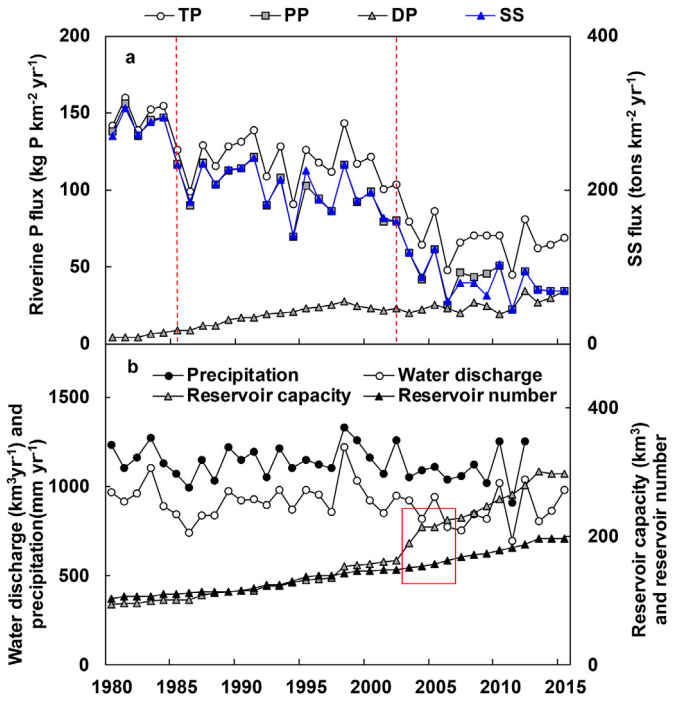

Fig. 5. (a) Temporal variations of P export and SS flux in Yangtze River and (b) historical trends of water discharge, precipitation, cumulative number and capacity of large dams/reservoirs (storage capacity >0.1 km^3) in the Yangtze River basin (red box indicates the period between the start of impounding water and the completion of the dam for the Three Gorges Dam). The red dash lines represent the start water impoundment for dam/reservoir group on the Jialing River (1986) and for the Three Gorge Dam (2003). (For interpretation of the references to colour in this figure legend, the reader is referred to the Web version of this article.)

Table 2
Correlations between riverine P export and NAPI and its components in Yangtze River basin, 1980–2015.

P forms	Regression equations	R^2	n
TP	$F_{TP} = -0.06NAPI + 207.26$	0.65**	36
	$F_{TP} = -0.09NAPI_A + 198.92$	0.61**	36
	$F_{TP} = -0.19NAPI_B + 220.01$	0.69**	36
	$F_{TP} = -0.09CF + 195.98$	0.60**	36
	$F_{TP} = -0.24NFFI + 236.55$	0.64**	36
	$F_{TP} = -40.40\ln(NFI) + 270.84$	0.71**	36
	$F_{TP} = -17.56SI + 183.94$	0.02	36
	$F_{TP} = -1.52APD + 232.58$	0.75**	36
PP	$F_{PP} = -0.07NAPI + 217.24$	0.78**	36
	$F_{TP} = -0.11NAPI_A + 207.15$	0.74**	36
	$F_{TP} = -0.25NAPI_B + 232.10$	0.81**	36
	$F_{PP} = -0.11CF + 203.58$	0.73**	36
	$F_{PP} = -0.31NFFI + 255.30$	0.76**	36
	$F_{PP} = -0.80NFI + 145.15$	0.85**	36
	$F_{PP} = -37.91SI + 256.74$	0.09	36
	$F_{PP} = -1.91APD + 245.97$	0.86**	36
DP	$F_{DP} = 1E\text{-}05NAPI^{1.92}$	0.85**	36
	$F_{TP} = 7E\text{-}05NAPI_A^{1.77}$	0.83**	36
	$F_{TP} = 2E\text{-}05NAPI_B^{2.16}$	0.84**	36
	$F_{DP} = 23.55\ln(CF) - 143.91$	0.85**	36
	$F_{DP} = 1E\text{-}06NFFI^{2.65}$	0.86**	36
	$F_{DP} = 10.80\ln(NFI) - 25.17$	0.81**	36
	$F_{DP} = 20.30SI - 72.59$	0.37**	36
	$F_{DP} = 32.35\ln(APD) - 123.45$	0.82**	36

CF is chemical fertilizer P input, NFFI is net food/feed P input, NFI is non-food P input, APD is atmospheric P deposition, SI is seed P input. **$p < 0.001$.

3.4. Modeling and forecasting riverine P fluxes

We developed regression models for predicting riverine P exports based on the relationships between riverine P fluxes and the driving factors identified above. First, $NAPI_A$ (nonpoint source potential) and $NAPI_B$ (point source potential) were independently evaluated to address the impact of contrasting P sources. Second, we used dam capacity (V, km^3) to address the contribution of legacy P sources given the strong positive relationship between V and net accumulated NAPI ($R^2 = 0.99$, $p < 0.001$; Chen et al., 2019). Third, climate and hydrology variables incorporated the natural temporal variability. The following DP and PP predictive model equations were selected after screening several model formulations based on

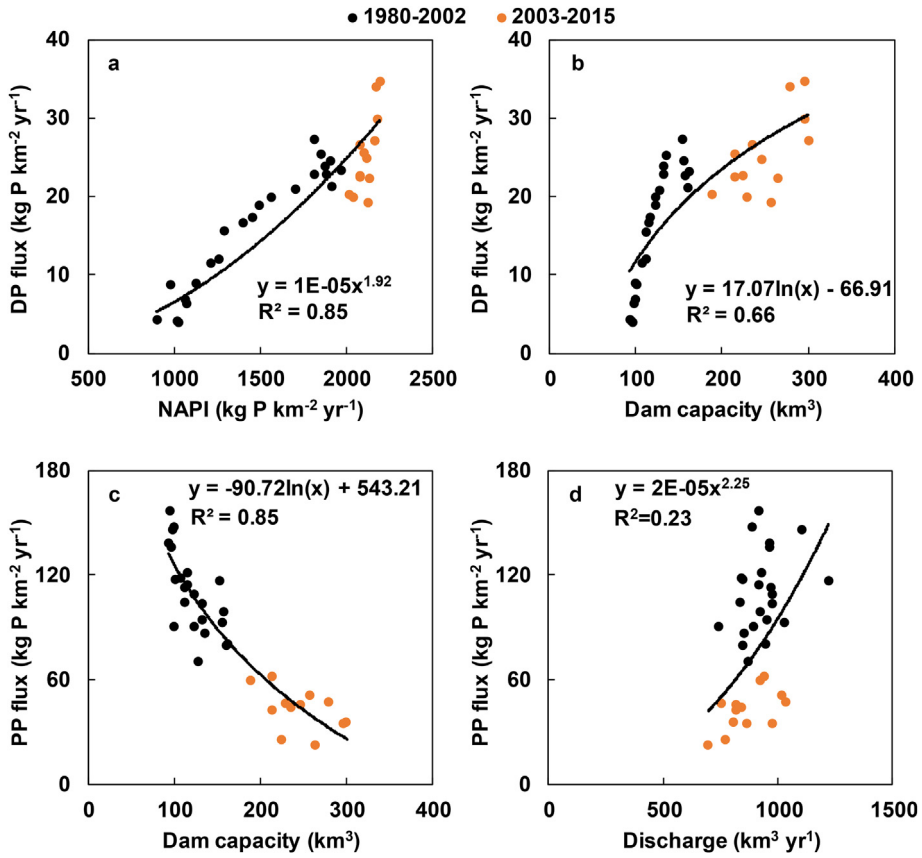

Fig. 6. Relationship between riverine DP flux and (a) NAPI and (b) dam capacity, and relationship between PP flux and (c) dam capacity and (d) discharge for the Yangtze River basin. An inflection point in 2003 appears related to completion of Three Gorges Dam.

simulation accuracy metrics (Table S8, SM, Part B):

$$F_{DP} = 0.009\ln VQ^{0.386}(NAPI_A^{0.461} + NAPI_B^{0.552}) - 17.599 \quad (3)$$

$$F_{PP} = 0.457Q^{0.501}(-6.441\ln V + 38.767) \quad (4)$$

Equation (3) accounted for 84% of the variation in annual riverine DP flux over the 1980–2015 period with a Nash-Sutcliffe efficiency coefficient (NSE) of 0.80 between modeled and observed values (Fig. 7b). Calibrated Eq. (4) explained 92% of the variation in annual riverine PP flux with a NSE of 0.92 (Fig. 7c). Annual riverine TP flux was considered the sum of DP and PP and explained 87% of the variation in annual riverine TP flux with a NSE of 0.84 (Fig. 7a). These strong model efficiency metrics verify the efficacy of the DP and PP predictive models. Thus, these model formulations provide a robust and reasonable performance for predicting annual riverine TP loads with relative errors ranging from −15.5 to 51.8% (average absolute error: 9.8%, Fig. 7a).

By setting average NAPI and water discharge at 2010–2015 levels and dam capacity in 2015 as baseline conditions, we forecasted riverine P exports for the 2016–2045 period based on regression equations (3) and (4). Four scenarios (e.g., developing, dam building, tackling A, and tackling B) were adopted to forecast future trends in NAPI and dam capacity (SM, Part C; Fig. 7c and d). Specifically, the "developing" scenario assumes a 55% increase of NAPI and 30% increase in dam capacity relative to 2015 (consistent with trends from 1980 to 2015). The "dam building" scenario incorporates a 30% increase in dam/reservoir capacity with constant NAPI relative to 2015. Under the "tackling A″ and "tackling B″ scenarios, $NAPI_A$ and $NAPI_B$ are projected to decrease 41% (~842 kg P km^{-2} yr^{-1}) and 39% (~439 kg P km^{-2} yr^{-1}), respectively.

Under the "developing" scenario, although riverine TP flux would decrease 16% due to a significant decrease in PP flux (~80% decrease), DP flux is predicted to increase by 50% in 2045 (Fig. 7). Despite the decrease of PP and TP fluxes, an increased DP (bioavailable P) flux could introduce considerable risks for eutrophication. Under the "dam building" scenario, riverine TP flux showed a considerable decrease (−37%) (Fig. 7a) along with decreased PP (−80%) and increased DP (+7%) fluxes (Fig. 7b and c). Under the "tackling A" scenario, riverine TP flux showed a considerable decrease (−8%) (Fig. 7a), along with a decrease in DP (−15%) flux. The "tackling B″ scenario projects a considerable decrease (−11%) in riverine TP flux, along with a decrease in DP (−22%) flux (Fig. 7a).

4. Discussion

4.1. Long-term fate of NAPI

Due to relatively high population density, livestock density and agricultural land proportion (Table 1), estimated average NAPI (1783 kg P km^{-2} yr^{-1} in 1985–2015) for YRB was significantly higher than the average NAPI reported for mainland China (465 kg P km^{-2} yr^{-1} in 2009, Han et al., 2013), US watersheds (~463 kg P km^{-2} yr^{-1} in 2007, Han et al., 2012), Baltic Sea watersheds (~250 kg P km^{-2} yr^{-1} in 1900–2013, McCrackin et al., 2018), and the St. Lawrence Basin (~230 kg P km^{-2} yr^{-1} in 1901–2011, Goyette et al., 2016). Although average NAPI for the entire YRB was lower than the Huaihe River basin, the adjacent watershed to the north (2700 kg P km^{-2} yr^{-1} for 2003–2010; Zhang et al., 2015),

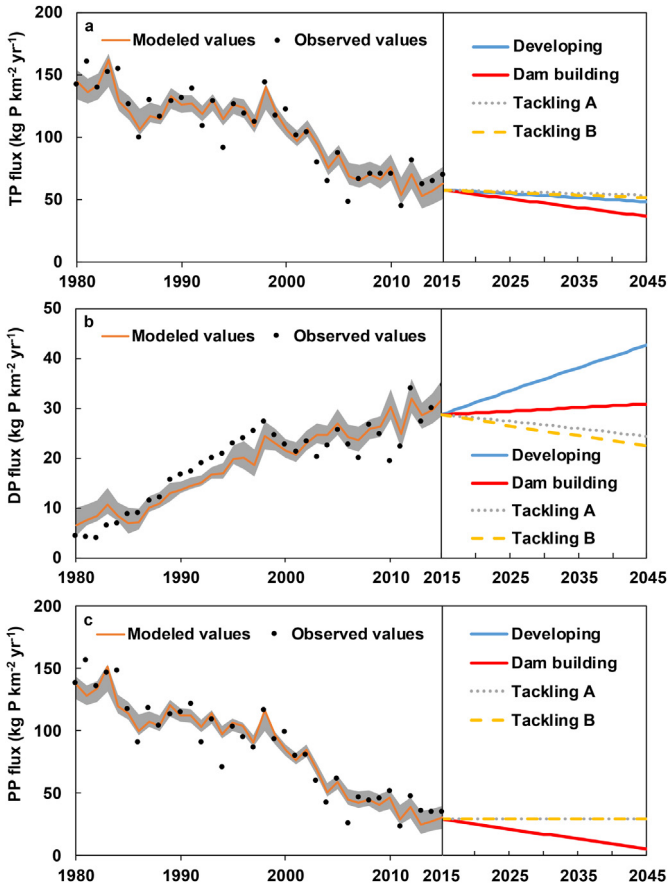

Fig. 7. Observed riverine (a) TP, (b) DP and (c) PP fluxes vs modeled values in the 1980–2015 study period; and predicted future (2016–2045) P changes under four future scenarios for the Yangtze River basin. Shaded area denotes 95% confidence interval for modeled riverine P fluxes.

NAPI in the downstream section of YRB (Fig. 3) was higher than that in the Huaihe River basin, indicating distinct NAPI hot spots within the YRB. Therefore, YRB is a global hotspot of anthropogenic P inputs and accumulation (Powers et al., 2016).

Assessing cumulative NAPI in the YRB, riverine export and retention in landscapes (e.g., soils and sediments) were the two major fates for the added P (Fig. S5, Russell et al., 2008). Estimated cumulative riverine TP export (3760 kg P km^{-2}) accounted for ~6% on average of total NAPI (~61050 kg P km^{-2}) over the 1980–2015 period, implying that the remaining ~94% of NAPI (~57290 kg P km^{-2}) was retained in the basin. Our estimated riverine P export percentage is within the range of 1.6–17% reported in previous studies (Russell et al., 2008; Chen et al., 2015; Goyette et al., 2016; Hong et al., 2017). Powers et al. (2016) estimated an average P accumulation in YRB of ~10 kg P ha^{-1} yr^{-1} during 1980–2010, which was relatively lower than our estimate (16 kg P ha^{-1} yr^{-1} during 1980–2015). This discrepancy results mainly because Powers et al. (2016) did not include food/feed and non-food P inputs in their analysis. Cropland soil and aquatic sediments are the likely major places for legacy P accumulation (Li et al., 2015; Maavara et al., 2015). Liu et al. (2018) reported a considerable increase of P accumulation (~7 times) in soils of the YRB from 1980 to 2010 (<0.2 to ~1.5 Tg P yr^{-1}; equivalent to ~80% of total accumulated P). This trend is consistent with elevated P accumulation rates for arable lands in China, which experienced increased levels of surplus P from ~1 to ~6 Tg P yr^{-1} from 1980 to 2010 (Li et al., 2015). In terms of P accumulation by dams/reservoirs in YRB, Maavara et al. (2015) estimated retention of ~1.8 Tg P in reservoirs, which accounted for 1.7% of total accumulated P during 1980–2015. The remaining ~18% of accumulated P may be retained in wetlands, lakes and rivers within the basin (Chen et al., 2018). Although small compared to P retained by soils (~80%), the P retained in water bodies maybe more easily transformed to DP providing a long-term P source for phytoplankton and macrophyte production (Zhou et al., 2013). Generally, these legacy P pools (soil and sediment) increase the risk of P loss to riverine transport if the accumulated P becomes mobilized by human activities or future changes in hydroclimate.

4.2. Riverine P transformations

The trends in long-term riverine P fluxes identified in this study (Fig. 2) are consistent with Xu et al. (2018) who reported a significant decrease of TP concentration in rivers (~65%) and lakes/reservoirs (~57%) in YRB during the 2006–2016 period. Zhou et al. (2013) also highlighted a considerable decrease of PP (~84%) and TP (~77%) fluxes from 1950 to 2011. Despite these decreasing trends, DP in the Yangtze River chronically exceeds the critical concentration of 0.05 mg P L^{-1} set to limit the risk of excessive algal growth (Li et al., 2010).

Over the study period, riverine P fluxes and forms changed remarkably in YRB (Fig. 5a). These P dynamics were regulated by changes in NAPI, dam/reservoir capacity and land cover/use (Figs. 5 and 6; Table 2). Specifically, riverine PP fluxes were more strongly affected by factors influencing transport processes than P input sources. Large-scale dam building is an important factor regulating SS and PP fluxes in the YRB (Dai et al., 2016; Yang et al., 2018). Riverine PP fluxes showed two periods with decreasing trends in the mid-1980s (>30% decrease compared to pre-dam period) and 2003–2006 (~40% decrease; Fig. 5a) associated with two stages of dam/reservoir building in the YRB since 1980. The considerable decrease in riverine PP fluxes associated with SS is attributed to a group of dams (capacity: 5.6 km^3) built on the Jialing River (a major tributary) during 1985–2002 (Fig. 5a; Yang et al., 2006), such as the Shengzhong (1.3 km^3) and Baozhusi (2.6 km^3) reservoirs. Since completion of Three Gorge Dam (39.3 km^3) in 2003, the reservoir intercepted ~170 Mt yr^{-1} sediments with an average interception efficiency of 75% (Hu et al., 2009). Thus, interception of sediment and associated P was greatly increased in reservoirs of the YRB (Maavara et al., 2015; Liu et al., 2018). At the global scale, increasing dam construction reduced riverine TP exports, with an estimated doubling of retained TP in reservoirs between 1970 and 2000, accounting for ~12% of the global riverine TP load in 2000 (Maavara et al., 2015).

Decreasing trends in riverine SS and PP fluxes are also attributable to improved soil and water conservation practices within the YRB. Soil and water conservation areas in the YRB reduced the area subject to high soil erosion potential by ~30% between 2002 and 2013 (Changjiang Water Resources Commission, 2016). Soil and water conservation areas in the YRB reached ~4 × 10^5 km^2 by 2015, with a ~5% increase in vegetative coverage from 1982 to 2015 (Qu et al., 2018) achieving a remarkable reduction in soil erosion and corresponding SS export (Yang et al., 2018).

We posit that the increasing trend for riverine DP fluxes results from elevated NAPI, dam-building, and legacy P pools (Figs. 2 and 5). Riverine DP flux was independent of rainfall and river discharge (Table 2), suggesting that point source pollution ($NAPI_B$) might be an important contributor of riverine DP (Fig. 7). Li et al. (2011) estimated that sewage discharge in YRB increased from 197 × 10^8 to 347 × 10^8 Mt between 1998 and 2015 (>75% increase). Previous modeling studies also suggested the importance of point sources to riverine P export in YRB, with estimates of 25–37% of DP flux in

2003 (Ding et al., 2010; Li et al., 2011) and 14% of TP flux in 2000 (Wang et al., 2011).

A considerable legacy P pool has accumulated in soils/sediments of the YRB where it may be mobilized/transformed to become an important DP source (Zhou et al., 2013). The buildup of legacy P in soils/sediments due to long-term excessive NAPI is susceptible to release as DP to surface waters (Chen et al., 2018). Organic matter mineralization within the water column and sediments, as well as redox-mediated release of PO_4^{3-} from iron (hydr)oxides in anoxic sediments may generate DP during reservoir impoundment (Ahearn et al., 2005; Maavara et al., 2017), facilitating the release of P from particulate forms. Therefore, despite significant reductions in PP and TP fluxes (Fig. 5a), the concomitant increase of bioavailable DP export contributes to downstream eutrophication. Increased water clarity associated with decreased SS elevates light penetration and the temperature of surface waters and sediments, which may further enhance microbial activities and the photo-release of dissolved organic matter and nutrients from particulate forms (He et al., 2016). Hypoxic water released by dams may further enhance redox transformations and release of DP from sediments in downstream channels (He et al., 2016). Our results revealed a decreasing P retention efficiency in the YRB since 2006 (Fig. S12), which we attribute to increasing P-saturation of soils/sediments (Chen et al., 2019). Increasing NAPI and decreasing P-retention efficiency lead to elevated riverine P export (especially DP), and thereby pose enhanced ecological risks to aquatic ecosystems (Beusen et al., 2016).

4.3. Efficacy and implications of the model for forecasting riverine P fluxes

The developed regression models Eqs. (3) and (4) incorporating contrasting P input sources, as well as hydrological and river regulation factors, demonstrated good accuracy for predicting annual riverine P fluxes (Fig. 7). The efficiency metrics ($R^2 = 0.84–0.92$; NSE = 0.80–0.92; relative error: 10–21%) for our regression-based models (Fig. 7) were comparable or superior to several previous lumped/mechanistic models for the YRB. Previous modeling efforts produced relative errors ranging from −66 to 115%, such as for the improved export coefficient model (−66 to 1% for year 2003, Ding et al., 2010), ENPS-LSB model (17.7% in 2000, Wang et al., 2011) and Global NEWS-DIP model (−39.2 to 114.7% for 1970–2003, Li et al., 2011). Efficiency metrics for our developed models were also comparable to previous NAPI-based models ($R^2 = 0.64–0.97$) for predicting riverine P fluxes in other watersheds (Russell et al., 2008; Hong et al., 2012, 2017; Chen et al., 2015, 2016a; Zhang et al., 2015; Goyette et al., 2016). In contrast to previous applications, this study validated model efficiencies by comparing the sum of modeled PP and DP fluxes to measured TP fluxes, providing a simple and effective approach for model validation. Considering the complexities of P biogeochemistry and transport processes at large spatial and temporal scales, our riverine P-export models established using long-term records (36 years) combined with the NAPI method were deemed robust with good accuracy.

This study highlights the role of dams/reservoirs in regulating P retention, transformation and export that must be considered in modeling riverine P fluxes (Ahearn et al., 2005; Zhou et al., 2013). Given the considerable number (>70,000) of large global dams/reservoirs and their continued construction, a large amount of P has been retained in reservoirs where it may be potentially transformed to more bioavailable forms (Maavara et al., 2015). Thus, our models provide a simple and effective tool for assessing long-term P dynamics and guiding development of P pollution control strategies for large river systems. Although the predictions are subject to considerable uncertainties in forecasting future P inputs and legacy P pools, the predicted results under the “developing” and “tackling B” scenarios roughly represent the upper (DP ≈ 0.08 mg L^{-1}) and lower (DP ≈ 0.04 mg L^{-1}) bounds for future riverine DP (most bioavailable form) exports/concentrations in response to anthropogenic activities and hydroclimate change. The predicted riverine P export bounds thereby provide a baseline for evaluating and adopting relevant watershed P management strategies.

4.4. Implications for watershed P management

Quantitative information on long-term NAPI and riverine P export is critical for optimizing watershed P management strategies (McCrackin et al., 2018). Considering the riverine P flux predicting models and forecasts, several remediation strategies are warranted for reducing P loading to surface waters. First, given the high contribution (>90%, Fig. 2) of fertilizer P input to nonpoint source pollution potential ($NAPI_A$), more attention should be paid to reduce chemical P fertilizer application and improve P-use efficiency in meeting crop yield demands (Chen et al., 2018), especially in the middle and lower reaches of the basin. Second, considering the increasing riverine DP flux (Fig. 7b) and the increasing point source pollution potential ($NAPI_B$, Fig. 2), it is important to improve collection and processing of animal and domestic wastewater (current treatment rates range from ~30 to ~70% in China; Hu et al., 2014) to reduce point source P pollution loading to surface waters. Third, as a considerable fraction of NAPI was retained as PP in soils and sediments trapped in reservoirs, optimized farm management practices (e.g., minimizing erosion, use of plants and microbial inoculants with high P extraction efficiency, precision P fertilizer management; Gaba et al., 2014) and interception and reuse of P from farmland runoff (e.g., riparian buffer strips, wetlands, irrigation water reuse; Macintosh et al., 2018; Chen et al., 2019) should be promoted to reduce the mobilization/transport of legacy P pools.

Despite watershed P management strategies, reduction of both N and P levels in the YRB is warranted to control eutrophication and harmful algal blooms (HABs). The NANI:NAPI molar ratio in the YRB was >8:1 during the past decades (Fig. S13, Chen et al., 2016b), which compares to a Redfield ratio of 16:1 (N:P) for marine algae. However, the dissolved inorganic nitrogen (DIN = NH_4+NO_3+NO_2) to DP molar ratio (DIN:DP) at Datong Station in the lower YRB showed a decreasing trend in the past decades (~430 in 1980 to ~120 in 2012), which may be related to differential transport and transformation processes for N and P (Alexander et al., 2008). The relatively high DIN:DP ratio in the Yangtze River implies ultimate P limitation for the exported water. As coastal and marine systems are typically N-limitation, the high DIN:DP coupled with decreasing silica (an essential element for diatom algae) export caused by river impoundments (Dai et al., 2011) could increase the prevalence of eutrophication and HABs in downstream and coastal areas (Liu et al., 2018). Therefore, comprehensive strategies should address decreasing both N and P riverine fluxes. In the YRB, chemical fertilizer (51% for NANI and 60% for NAPI) and food/feed inputs (26% for NANI and 31% for NAPI) are the largest nutrient inputs. Thus, management strategies that target increased fertilizer-use efficiency and improved sewage disposal/reuse will be most effective at addressing both riverine N and P fluxes.

5. Conclusion

This study accomplished the first long-term spatio-temporal analysis of anthropogenic P inputs and historical riverine P exports for the YRB in 1980–2015. NAPI increased ~1.4-fold from 1980 to 2015 driven primarily by increases in fertilizer P input (52–65%)

and net food/feed P inputs (27–39%). NAPI and its components showed a trend of increasing from western to eastern China, with the highest rates of NAPI increase occurring in the upstream and midstream segments of the YRB. NAPI dynamics were strongly related to population density, livestock density and agricultural land proportion. Despite a significant decrease of riverine TP, PP and SS fluxes, riverine DP flux increased 7-fold over the study period. More than 94% of NAPI was retained in the basin, which leads to accumulation of large legacy P pools that could be mobilized with changes in land use or climate change. Riverine TP and PP flux dynamics in the YRB were more strongly affected by factors influencing transport processes rather than P sources. In contrast, riverine DP flux appears to be determined by P sources ($NAPI_A$ and $NAPI_B$) and factors influencing transport processes (i.e., increasing reservoir impoundment and vegetation coverage). Multiple regression models incorporating $NAPI_A$, $NAPI_B$, dam storage capacity and water discharge were highly effective in explaining inter-annual variability in riverine DP and PP fluxes; these results were verified by the strong agreement between estimated TP (DP + PP) flux and measured TP values. This study identified a critical need to better understand the role of river regulation on P transformation mechanisms that have resulted in continuously increasing concentrations of more bioavailable DP during the study period.

Declaration of competing interest

The authors declare that they have no known competing financial interests or personal relationships that could have appeared to influence the work reported in this paper.

Acknowledgement

This work was supported by the National Key Research and Development Program of China (2017YFD0800101), National Natural Science Foundation of China (51679210 and 41877465), and Zhejiang Provincial Natural Science Foundation of China (LR19D010002).

Appendix A. Supplementary data

Supplementary data to this article can be found online at https://doi.org/10.1016/j.watres.2020.115779.

References

Ahearn, D.S., Sheibley, R.W., Dahlgren, R.A., 2005. Effect of river regulation on water quality in the Sierra Nevada, California. River Res. Appl. 21, 651–670.
Alexander, R.B., Smith, R.A., Schwarz, G.E., Boyer, E.W., Nolan, J.V., Brakebill, J.W., 2008. Differences in phosphorus and nitrogen delivery to the Gulf of Mexico from the Mississippi River basin. Environ. Sci. Technol. 42, 822–830.
Beusen, A.H.W., Bouwman, A.F., Van Beek, L.P.H., Mogollon, J.M., Middelburg, J.J., 2016. Global riverine N and P transport to ocean increased during the 20th century despite increased retention along the aquatic continuum. Biogeosciences 13, 2441–2451.
Chai, C., Yu, Z.M., Shen, Z.L., Song, X.X., Cao, X.H., Yao, Y., 2009. Nutrient characteristics in the Yangtze River estuary and the adjacent east China sea before and after impoundment of the three Gorges dam. Sci. Total Environ. 407 (16), 4687–4695.
Chen, D.J., Hu, M.P., Guo, Y., Dahlgren, R.A., 2015. Influence of legacy phosphorus, land use, and climate change on anthropogenic phosphorus inputs and riverine export dynamics. Biogeochemistry 123 (1–2), 99–116.
Chen, D.J., Hu, M.P., Wang, J.H., Guo, Y., Dahlgren, R.A., 2016a. Factors controlling phosphorus export from agricultural/forest and residential systems to rivers in eastern China, 1980-2011. J. Hydrol. 533, 53–61.
Chen, F., Hou, L.J., Liu, M., Zheng, Y.L., Yin, G.Y., Lin, X.B., Li, X.F., Zong, H.B., Deng, F.Y., Gao, J., Jiang, X.F., 2016b. Net anthropogenic nitrogen inputs (NANI) into the Yangtze River basin and the relationship with riverine nitrogen export. J. Geophys. Res.-Biogeo. 121 (2), 451–465.
Chen, D.J., Shen, H., Hu, M.P., Wang, J.H., Zhang, Y.F., Dahlgren, R.A., 2018. Legacy nutrient dynamics at the watershed scale: principles, modeling, and implications. Adv. Agron. 149, 237–313.
Chen, D., Zhang, Y., Shen, H., Yao, M., Hu, M., Dahlgren, R.A., 2019. Decreased buffering capacity and increased recovery time for legacy phosphorus in a typical watershed in eastern China between 1960 and 2010. Biogeochemistry 144 (3), 273–290.
Changjiang Water Resources Commission, 2016. Water and Soil Conservation Bulletin of the Yangtze River Basin during 2006-2015. Data available at: http://www.cjw.gov.cn/zwzc/bmgb/2017ngb/24715.html. (Accessed 25 March 2020).
Dai, Z.J., Du, J.Z., Zhang, X.L., Su, N., Li, J.F., 2011. Variation of riverine material loads and environmental consequences on the Changjiang (Yangtze) estuary in recent decades (1955-2008). Environ. Sci. Technol. 45 (1), 223–227.
Dai, Z.J., Fagherazzi, S., Mei, X.F., Gao, J.J., 2016. Decline in suspended sediment concentration delivered by the Changjiang (Yangtze) river into the east China sea between 1956 and 2013. Geomorphology 268, 123–132.
Ding, X.W., Shen, Z.Y., Hong, Q., Yang, Z.F., Wu, X., Liu, R.M., 2010. Development and test of the export coefficient model in the upper reach of the Yangtze River. J. Hydrol. 383 (3–4), 233–244.
Eiriksdottir, E.S., Oelkers, E.H., Hardardottir, J., Gislason, S.R., 2017. The impact of damming on riverine fluxes to the ocean: a case study from Eastern Iceland. Water Res. 113, 124–138.
Gaba, S., Lescourret, F., Boudsocq, S., Enjalbert, J., Hinsinger, P., Journet, E.P., Navas, M.L., Wery, J., Louarn, G., Malézieux, E., Pelzer, E., Prudent, M., Ozier-Lafontaine, H., 2014. Multiple cropping systems as drivers for providing multiple ecosystem services: from concepts to design. Agron. Sustain. Dev. 35, 607–623.
Goyette, J.O., Bennett, E.M., Howarth, R.W., Maranger, R., 2016. Changes in anthropogenic nitrogen and phosphorus inputs to the St. Lawrence sub-basin over 110 years and impacts on riverine export. Global Biogeochem. Cycles 30 (7), 1000–1014.
Goyette, J.O., Bennett, E.M., Maranger, R., 2018. Low buffering capacity and slow recovery of anthropogenic phosphorus pollution in watersheds. Nat. Geosci. 11, 921–925.
Gupta, H., Kao, S.J., Dai, M.H., 2012. The role of mega dams in reducing sediment fluxes: a case study of large Asian rivers. J. Hydrol. 464–465, 447–458.
Han, H., Allan, J.D., Bosch, N.S., 2012. Historical pattern of phosphorus loading to Lake Erie watersheds. J. Great Lake. Res. 38, 289–298.
Han, H., Bosch, N., Allan, J.D., 2011. Spatial and temporal variation in phosphorus budgets for 24 watersheds in the Lake Erie and Lake Michigan basins. Biogeochemistry 102 (1–3), 45–58.
Han, Y.G., Yu, X.X., Wang, Y.Q., Wang, C.Z., Wang, X.X., Tian, J.X., Xu, L., 2013. Net anthropogenic phosphorus inputs (NAPI) index application in Mainland China. Chemosphere 90 (2), 329–337.
He, W., Chen, M., Schlautman, M.A., Hur, J., 2016. Dynamic exchanges between DOM and POM pools in coastal and inland aquatic ecosystems: a review. Sci. Total Environ. 551, 415–428.
Hong, B., Swaney, D.P., McCrackin, M., Svanbäck, A., Humborg, C., Gustafsson, B., Yershova, A., Pakhomau, A., 2017. Advances in NANI and NAPI accounting for the Baltic drainage basin: spatial and temporal trends and relationships to watershed TN and TP fluxes. Biogeochemistry 133 (3), 245–261.
Hong, B., Swaney, D.P., Mörth, C.M., Smedberg, E., Hägg, H.E., Humborg, C., Howarth, R.W., Bouraoui, F., 2012. Evaluating regional variation of net anthropogenic nitrogen and phosphorus inputs (NANI/NAPI), major drivers, nutrient retention pattern and management implications in the multinational areas of Baltic Sea basin. Ecol. Model. 227, 117–135.
Hu, F., Tan, D., Lazareva, I., 2014. 8 Facts on China's Wastewater. China Water Risk. http://www.chinawaterrisk.org/resources/analysis-reviews/8-facts-on-china-wastewater/. (Accessed 21 October 2019).
Hu, B.Q., Yang, Z.S., Wang, H.J., Sun, X.X., Bi, N.S., Li, G.G., 2009. Sedimentation in the three Gorges dam and the future trend of Changjiang (Yangtze River) sediment flux to the sea. Hydrol. Earth Syst. Sci. 13 (11), 2253–2264.
Li, H.G., Liu, J., Li, G.H., Shen, J.B., Bergström, L., Zhang, F.S., 2015. Past, present, and future use of phosphorus in Chinese agriculture and its influence on phosphorus losses. Ambio 44 (2), 274–285.
Li, X.Y., Yang, L.B., Yan, W.J., 2011. Model analysis of dissolved inorganic phosphorus exports from the Yangtze River to the estuary. Nutrient Cycl. Agroecosyst. 90 (1), 157–170.
Li, S.S., Yuan, Z.W., Bi, J., Wu, H.J., 2010. Anthropogenic phosphorus flow analysis of Hefei City, China. Sci. Total Environ. 408 (23), 5715–5722.
Liu, X.C., Beusen, A.H.W., Van Beek, L.P.H., Mogollón, J.M., Ran, X.B., Bouwman, A.F., 2018. Exploring spatiotemporal changes of the Yangtze River (Changjiang) nitrogen and phosphorus sources, retention and export to the east China sea and yellow sea. Water Res. 142, 246–255.
Maavara, T., Lauerwald, R., Regnier, P., Cappellen, P.V., 2017. Global perturbation of organic carbon cycling by river damming. Nat. Commun. 8, 15347.
Maavara, T., Parsons, C.T., Ridenour, C., Stojanovic, S., Dürr, H.H., Powley, H.R., Cappellen, P.V., 2015. Global phosphorus retention by river damming. Proc. Natl. Acad. Sci. U.S.A. 112 (51), 15603–15608.
Macintosh, K.A., Mayer, B.K., McDowell, R.W., Powers, S.M., Baker, L.A., Boyer, T.H., Rittmann, B.E., 2018. Managing diffuse phosphorus at the source versus at the sink. Environ. Sci. Technol. 52 (21), 11995–12009.
McCrackin, M.L., Muller-Karulis, B., Gustafsson, B.G., Howarth, R.W., Humborg, C., Svanbäck, A., Swaney, D.P., 2018. A century of legacy phosphorus dynamics in a large drainage basin. Global Biogeochem. Cycles 32 (7), 1107–1122.
Powers, S.M., Bruulsema, T.W., Burt, T.P., Chan, N.L., Elser, J.J., Haygarth, P.M.,

Howden, N.J.K., Jarvie, H.P., Lyu, Y., Peterson, H.M., Sharpley, A.N., Shen, J.B., Worrall, F., Zhang, F.S., 2016. Long-term accumulation and transport of anthropogenic phosphorus in three river basins. Nat. Geosci. 9, 353–356.
Qu, S., Wang, L.C., Lin, A.W., Zhu, H.J., Yuan, M.X., 2018. What drives the vegetation restoration in Yangtze River basin, China: climate change or anthropogenic factors? Ecol. Indicat. 90, 438–450.
Russell, M.J., Weller, D.E., Jordan, T.E., Sigwart, K.J., Sullivan, K.J., 2008. Net anthropogenic phosphorus inputs: spatial and temporal variability in the Chesapeake Bay region. Biogeochemistry 88 (3), 285–304.
Shen, Z.Y., Chen, L., Ding, X.W., Hong, Q., Liu, R.M., 2013. Long-term variation (1960–2003) and causal factors of non-point-source nitrogen and phosphorus in the upper reach of the Yangtze River. J. Hazard Mater. 252–253, 45–56.
Stackpoole, S.M., Stets, E.G., Sprague, L.A., 2019. Variable impacts of contemporary versus legacy agricultural phosphorus on US river water quality. Proc. Natl. Acad. Sci. U.S.A. 116 (41), 20562–20567.
Steffen, W., Richardson, K., Rockström, J., Cornell, S.E., Fetzer, I., Bennett, E.M., Biggs, R., Carpenter, S.R., De Vries, W., De Wit, C.A., Folke, C., 2015. Planetary boundaries: guiding human development on a changing planet. Science 347 (6223), 1259855.
Tong, Y.D., Zhao, Y., Zhen, G.C., Chi, J., Liu, X.H., Lu, Y.R., Wang, X.J., Yao, R.H., Chen, J.Y., Zhang, W., 2015. Nutrient loads flowing into coastal waters from the main rivers of China (2006–2012). Sci. Rep. 5 (1), 16678.
Vitousek, P.M., Porder, S., Houlton, B.Z., Chadwick, O.A., 2010. Terrestrial phosphorus limitation: mechanisms, implications, and nitrogen–phosphorus interactions. Ecol. Appl. 20, 5–15.
Wang, H., Yang, Z., Wang, Y., Saito, Y., Liu, J.P., 2008. Reconstruction of sediment flux from the Changjiang (Yangtze River) to the sea since the 1860s. J. Hydrol. 349 (3), 318–332.
Wang, X., Hao, F.H., Cheng, H.G., Yang, S.T., Zhang, X., Bu, Q.S., 2011. Estimating non-point source pollutant loads for the large-scale basin of the Yangtze River in China. Environ. Earth Sci. 63 (5), 1079–1092.
Xu, S., 2017. Temporal and Spatial Variation Characteristics of Land Use and its Runoff Effect in the Nearly 35 Yangtze River Basin. Thesis. ZhengZhou University.
Xu, Y.X., Wu, X., Lu, R., Yang, W.J., Zhao, Y., 2018. Total phosphorus pollution, countermeasures and suggestions of the Yangtze River economic belt. Chin. J. Environ. Manage. 10 (1), 70–74 (in Chinese).
Yang, Z.S., Wang, H.J., Saito, Y., Milliman, J.D., Xu, K., Qiao, S., Shi, G., 2006. Dam impacts on the Changjiang (Yangtze) river sediment discharge to the sea: the past 55 years and after the three Gorges dam. Water Resour. Res. 42, W04407. https://doi.org/10.1029/2005WR003970.
Yang, Z., Yang, S.L., Yang, H.F., Xu, K.H., Milliman, J.D., Wang, H., Chen, Z., Zhang, C.Y., 2018. Human impacts on sediment in the Yangtze River: a review and new perspectives. Global Planet. Change 162, 8–17.
Yuan, Z.W., Jiang, S.Y., Sheng, H., Sheng, H., Liu, X., Hua, H., Liu, X.W., Zhang, Y., 2018. Human perturbation of the global phosphorus cycle: changes and consequences. Environ. Sci. Technol. 52 (5), 2438–2450.
Zhang, W.S., Swaney, D.P., Hong, B., Howarth, R.W., Han, H., Li, X.Y., 2015. Net anthropogenic phosphorus inputs and riverine phosphorus fluxes in highly populated headwater watersheds in China. Biogeochemistry 126 (3), 269–283.
Zhao, Y.F., Zou, X.Q., Liu, Q., Yao, Y.L., Li, Y.L., Wu, X.W., Wang, C.L., Yu, W.W., Wang, T., 2017. Assessing natural and anthropogenic influences on water discharge and sediment load in the Yangtze River, China. Sci. Total Environ. 607, 920–932.
Zhou, J.J., Zhang, M., Lu, P.Y., 2013. The effect of dams on phosphorus in the middle and lower Yangtze River. Water Resour. Res. 49 (6), 3659–3669.